ChemPhysChem

A nuclear configuration interaction approach to study nuclear spin effects: an application to ortho- and para-3He2@C60

--Manuscript Draft--

Manuscript Number:	cphc.202300498
Article Type:	Research Article
Corresponding Author:	Andrés Reyes, Ph.D. Universidad Nacional de Colombia Bogota, COLOMBIA
Corresponding Author E-Mail:	areyesv@unal.edu.co
Order of Authors (with Contributor Roles):	Félix Moncada, PhD
	William Quintero, MSc.
	Edwin Posada, PhD
	Lars G.M. Pettersson, PhD
	Andrés Reyes, Ph.D.
Keywords:	Nuclear quantum effects; Ab-initio calculations; Confined atoms; Endohedral fullerenes; Nuclear spin effects
Manuscript Classifications:	Ab initio calculations; Computational chemistry; Isotope effects; Molecular modeling; Quantum Chemistry
Suggested Reviewers:	Rita Prosmiti rita@iff.csic.es Expertise in nuclear spin effects
	Alvaro Valdes avaldesl@unal.edu.co Expertise in nuclear spin effects
	Maria Pilar de Lara pilar.delara.castells@csic.es Expertise in nuclear spin effects
	Pablo Villarreal p.villarreal@csic.es Expertise in nuclear spin effects
	Gabriel Merino gabriel.merino2@gmail.com Expertise in electronic structure calculations of confined systems
	Roberto Flores-Moreno Roberto.FloresMoreno.QT@gmail.com Expertise in electronic structure calculations of confined systems
Opposed Reviewers:	
Abstract:	We introduce a non-orthogonal configuration interaction approach to investigate nuclear quantum effects on energies and densities of confined fermionic nuclei. The Hamiltonian employed draws parallels between confined systems and many-electron atoms, where effective non-Coulombic potentials represent the interactions of the trapped particles. One advantage of this method is its generality, as it offers the potential to study nuclear quantum effects of various confined species affected by effective isotropic or anisotropic potentials. As a first application, we analyze the quantum states of two 3He atoms encapsulated in C60. At the Hartree-Fock level, we observe the breaking of spin and spatial symmetries. To ensure wavefunctions with the correct symmetries, we mix the broken-symmetry Hartree-Fock states within the non-orthogonal configuration interaction expansion.

	Our proposed approach predicts singly and triply degenerate ground states for the singlet (para-3He2@C60) and triplet (ortho-3He2@C60) nuclear spin configurations, respectively. The ortho-3He2@C60 ground state is 5.69 cm-1 higher in energy than the para-3He2@C60 ground state. The nuclear densities obtained for these states exhibit the icosahedral symmetry of the C60 embedding potential. Importantly, our calculated densities and energies align perfectly with the expected symmetries and energies obtained with a simple quantum harmonic oscillator plus rigid rotor model of the 3He2@C60 system.
Author Comments:	Doctor Rita Prosmiti Guest Editor ChemPhysChem Dear Editor, We are delighted to submit our contribution for the special edition commemorating the remarkable achievements of Prof. Pablo Villarreal. Our submission aligns closely with the research interests and areas of expertise of Prof. Villarreal. It is truly an honor for us to be invited to contribute to this special edition of ChemPhysChem: "Computational modeling: up-to-date approaches and cutting-edge applications from clusters, nanostructures to bulk systems". Nuclear spin effects (NSEs) play an important role in the structural and spectroscopic properties of systems containing multiple identical fermionic nuclei. Quantum approaches are commonly employed to study NSEs and describe the quantum nature of nuclei. NSEs have been extensively investigated in systems with identical hydrogen nuclei, as well as helium. The strategies developed for helium systems have been inspired by electronic structure methods. It has been observed that the Hartree-Fock (HF) description fails to provide accurate predictions, particularly for low-spin wavefunctions. However, these predictions can be improved by employing multiconfigurational schemes, such as configuration interaction (CI) and multiconfigurational time-dependent Hartree (MCTDH) methods. However, these schemes have limitations in terms of the number of particles and degrees of freedom they can handle, as well as the representation of the Hamiltonian and effective potentials. In this contribution, we introduce a non-Coulomb non-orthogonal CI scheme to overcome these limitations. Our method offers lower scaling than CI and MCTDH methods, and its generality enables the use of a Hamiltonian written in Cartesian coordinates to handle an arbitrary number of quantum nuclei. We have implemented this method in the openLOWDIN code, which is freely available at https://doi.org/10.5281/zenodo.8125056 As a preliminary test of our approach, we analyze the NSEs on the wavefunctions and energies of two helium atoms trapped in C60. Our results are compared to those obtained from a simplified harmonic oscillator plus rigid rotor (HO+RR) model. While the NC-HF results exhibit incorrect energy and wavefunction symmetry, these predictions are corrected at the NC-NOCI level. Remarkably, our NC-NOCI predictions align well with those of the simplified HO+RR model. Further analysis of the densities and excited state level splitting confirms the superiority of NC-NOCI over HO+RR in capturing the anisotropy of the confining potential. We believe that our findings significantly contribute to the understanding of NSEs in confined systems and offer a valuable methodological advancement. Sincerely, Prof. Andrés Reyes Quantum and Computational Chemistry group Universidad Nacional de Colombia Av. Cra 30 #45-03, Bogotá, Colombia Email: areyesv@unal.edu.co Telephone: +57 601315000 Ext. 10616
Section/Category:	Special Collection: Pablo Villarreal Herrán Festschrift

Additional Information:	
Question	**Response**
Do you agree to comply with the legal and ethical responsibilities outlined in the journal's Notice to Authors?	Yes
Has a previous version of this manuscript been submitted to this journal?	No
Is this manuscript, or part of it, currently under consideration elsewhere?	No
Is this manuscript, or part of it, published, posted, or in press? This includes content posted on preprint servers (preprint guidelines) or published as part of a thesis.	No
Please provide us with information about the history of your manuscript, including previous submissions, transfers, or prior versions:	This manuscript present a new approach we have been developing in the last two years. To demonstrate the proposed method capabilities, we selected the endohedral complex of two helium atoms inside C60. This system was studied previously with a less accurate approach in the master's thesis of one of the authors (William Quintero). These previous results served as a guideline for the results presented in the manuscript.
Do you or any of your co-authors have a conflict of interest to declare?	No
Does the research described in this manuscript include animal experiments?	No
Does the research described in this manuscript include human research participants (including for experiments with sensors or wearable technologies) or tissue samples from human subjects (including blood or sweat)?	No

A nuclear configuration interaction approach to study nuclear spin effects: an application to *ortho*- and *para*-$^3He_2@C_{60}$

Félix Moncada,[a,d] William Quintero,[b,d] Edwin Posada,[c,d] Lars G.M. Pettersson,[a] Andrés Reyes*[d]

Special Collection: Pablo Villarreal Herrán Festschrift

We introduce a non-orthogonal configuration interaction approach to investigate nuclear quantum effects on energies and densities of confined fermionic nuclei. The Hamiltonian employed draws parallels between confined systems and many-electron atoms, where effective non-Coulombic potentials represent the interactions of the trapped particles. One advantage of this method is its generality, as it offers the potential to study the nuclear quantum effects of various confined species affected by effective isotropic or anisotropic potentials.

As a first application, we analyze the quantum states of two ^3He atoms encapsulated in C_{60}. At the Hartree-Fock level, we observe the breaking of spin and spatial symmetries. To ensure wavefunctions with the correct symmetries, we mix the broken-symmetry Hartree-Fock states within the non-orthogonal configuration interaction expansion.

Our proposed approach predicts singly and triply degenerate ground states for the singlet (*para*$-^3He_2@C_{60}$) and triplet (*ortho*$-^3He_2@C_{60}$) nuclear spin configurations, respectively. The *ortho*$-^3He_2@C_{60}$ ground state is 5.69 cm^{-1} higher in energy than the *para*$-^3He_2@C_{60}$ ground state. The nuclear densities obtained for these states exhibit the icosahedral symmetry of the C_{60} embedding potential. Importantly, our calculated densities and energies align perfectly with the expected symmetries and energies obtained with a simple quantum harmonic oscillator plus rigid rotor model of the $^3He_2@C_{60}$ system.

Introduction

Nuclear quantum effects span a variety of phenomena, including zero-point energy, molecular vibrations, tunneling, and isotope effects.[1–3] These effects play a fundamental role in diverse disciplines, such as chemistry, biology, physics, and materials science. The study of nuclear quantum effects is crucial as it permits attaining a more accurate description and prediction of atomic, molecular, and condensed matter behavior.[4–10]

In contrast, certain nuclear quantum effects, specifically nuclear spin effects (NSEs), have a more subtle influence on the physical properties of matter.[11,12] Still, these NSEs play a crucial role in techniques such as nuclear magnetic resonance[13] and electron paramagnetic resonance,[14] which are widely employed for exploring molecular structure and properties. Similarly, accurately assigning rovibrational spectroscopic measurements depends on the proper understanding of NSEs.[15] Nuclear spin multiplicity influences the energy separation of quantum states. For instance, the rovibrational spectra of molecular hydrogen display an energy splitting of 118.9 cm^{-1} between the ground states of *ortho*-H_2 (*o*-H_2, with triplet H spin configuration) and *para*-H_2 (*p*-H_2, with singlet H spin configuration).[16] Similar energy splittings have been observed for the two nuclear spin isomers of water in the gas phase. Here, the ground state of *ortho*-water exhibits an energy 23.8 cm^{-1} higher than that of *para*-water.[17]

Nuclear spin effects extend beyond hydrogen-containing systems and can impact the properties of systems comprising multiple identical nuclei[18]. For instance, numerous investigations on pure and doped nanoclusters comprising ^3He and ^4He, have analyzed how different helium nuclear spin configurations affect their spectroscopic properties and superfluidity.[19–22] Furthermore, the experimental reports on doped clusters reveal that He atoms are brought closer together by condensation on molecules such as OCS[23], SF_6[24] or aromatic hydrocarbons[25].

Alternatively, the proximity of He atoms can be enforced by confining them within a molecular cage, such as a fullerene. Experimental results have demonstrated the presence of one and two helium atoms trapped inside fullerenes using spectroscopic techniques.[26–29]

Numerous theoretical investigations employing molecular mechanics and electronic structure approaches have analyzed various phenomena exhibited in systems with one and two He atoms trapped within C_{60}.[30–35] In particular, it has been shown that helium atoms within C_{60} exhibit a lower rotational barrier compared to other noble gases, indicating their relatively unrestricted motion within the cage.[36,37] Molecular dynamics simulations have also been utilized to incorporate the effects of temperature and analyze the classical distribution of nuclei.[38] Nevertheless, these studies

[a] Department of Physics, AlbaNova University Center, Stockholm University, Stockholm, Sweden

[b] Doctorado en Fisicoquímica Molecular, Universidad Andres Bello, Santiago de Chile, Chile

[c] Institute for Computational Molecular Science, Temple University, Philadelphia, PA, USA.

[d] Department of Chemistry, Universidad Nacional de Colombia, Av. Cra 30 45–03, Bogotá, Colombia
E-mail: areyesv@unal.edu.co

have overlooked the quantum nature of nuclei, resulting in the omission of analyses regarding the impact of NSEs on system properties.

Here, our primary objective is to develop a systematic Non-Coulombic (NC) Non-Orthogonal Configuration Interaction (NOCI) method to analyze NSEs in systems containing multiple identical nuclei. The NOCI approach has a lower formal scaling than full configuration interaction (FCI) and has been used in regular electronic structure [39–41] and nuclear plus electronic structure calculations [42] for systems where the Hartree-Fock (HF) method breaks the spin or spatial symmetry to lower the energy. It has been observed that by taking a linear combination of these broken-symmetry HF solutions, the NOCI can restore the static correlation and recover the correct symmetry of the wavefunction. [41] The proposed NC-NOCI method allows us to study NSEs on the quantization of nuclear states without the need to consider translational, rotational, and vibrational separations of the nuclear states. Furthermore, the systematic nature of the NC-NOCI approach makes it applicable for analyzing the quantum states of particles or pseudo-particles trapped in cavities of diverse shapes.

As a first application of our NC-NOCI approach, we calculate the nuclear wavefunctions and energies of two ^{3}He atoms (referred to as He hereafter) confined in C_{60} ($He_2@C_{60}$). This system exhibits nuclear spin isomerism, forming either *para*$-He_2@C_{60}$ (*p*-$He_2@C_{60}$) or *ortho*$-He_2@C_{60}$ (*o*-$He_2@C_{60}$) with singlet or triplet spin configurations, respectively. Therefore, NSEs may impact the He_2 structure and dynamic behavior. When applied to $He_2@C_{60}$, our approach decouples the degrees of freedom of C_{60} from those of the encapsulated He atoms. Furthermore, the He atoms are treated as dressed nuclei. This approach draws inspiration from electronic structure methods. Under this setting, we construct an effective Hamiltonian that considers He dressed nuclei as interacting quantum waves embedded in an external field generated by the carbon atoms. Equivalent effective Hamiltonians have been employed to study He clusters formed around molecules, [43–53] and inside carbon nanotubes [54].

The structure of the paper is as follows: In the Theoretical and Computational Aspects section, we present the proposed NC-NOCI approach and provide details of the numerical simulations. In the Results and Discussion section, we present the energies and densities obtained for two helium atoms trapped in C_{60}. Finally, in the Conclusions section, we provide final remarks summarizing the findings of this study.

Theoretical and Computational Aspects

From a quantum perspective, the calculation of the total wavefunction of two He atoms confined within C_{60} involves considering the degrees of freedom of 62 nuclei and 364 electrons.

Previous related studies have demonstrated that the dimensionality of the confined system can be significantly reduced by exploiting the minimal coupling between the motions of the confined species and those of C_{60} [55–61]. Based on this approximation, the degrees of freedom of He_2 and C_{60} can be adiabatically separated. The dimensionality can be further reduced by recognizing that He_2 does not form chemical bonds with the walls of C_{60} or with each other. As a result, each confined ^{3}He atom can be treated as a dressed nucleus, possessing a formal charge of 0 and a nuclear spin $s = 1/2$. The interactions between the He atoms and with the walls of C_{60} are accounted for through the utilization of effective potentials.

Due to the fermionic nature of He nuclei, approximate solutions of the time-independent Schrödinger equation, $\hat{H}\Psi = E\Psi$, can be obtained within an HF framework. This approach is analogous to the one utilized in studies of doped He clusters [43,45–49]. In this context, the He wavefunction, Ψ^{He}, is represented by a Slater determinant composed of He spin-orbitals. It has been found that at the HF level, only high-spin configurations are properly described, whereas low-spin configurations must be described with a multiconfigurational approach. [53] To overcome this limitation of the HF method and achieve an enhanced physical description, several dressed He nuclei studies have employed the FCI level and related multiconfigurational schemes [48,50–54].

The confined $^3He_2$ system can exist in singlet ($S = 0$, *para*-$^3He_2$) or in triplet ($S = 1$, *ortho*-$^3He_2$) nuclear spin state. In the case of *para*-$^3He_2$ (also called *p*-He_2), the quantum statistics is properly accounted for by antisymmetrizing the spin component of the nuclear wavefunction. Consequently, the orbital part is symmetric, leading to doubly occupied orbitals when employing a single-determinant representation. It is important to note that any other choice of singly occupied orbitals would result in spin contamination. In contrast, for *ortho*-He_2 (also called *o*-He_2), antisymmetrization occurs in the orbital part, where two orbitals are singly occupied. Therefore, when employing a single-determinant representation, the spin component must be symmetric.

Non-Coulombic Non-Orthogonal Configuration Interaction (NC-NOCI)

To capture the quantum behavior of identical encapsulated nuclei, we develop a Hamiltonian analogous to the electronic molecular Hamiltonian under the Born-Oppenheimer approximation. In this formulation, the nuclei of interest are treated as quantum particles, analogous to electrons, while the atoms comprising the encapsulating cage are considered fixed point-like particles. As a result, this Hamiltonian incorporates the nuclear kinetic energy, as well as the potential energy arising from the nucleus-nucleus and nucleus-cage interactions, expressed through effective pairwise potentials

$$\hat{H} = -\sum_{i}^{N_q} \frac{\nabla_i^2}{2m_q} + \sum_{i}^{N_q}\sum_{I}^{N_p} \hat{V}_{qp}(\mathbf{r}_i - \mathbf{R}_I) + \sum_{i}^{N_q}\sum_{j>i}^{N_q} \hat{V}_{qq}(\mathbf{r}_i - \mathbf{r}_j). \tag{1}$$

Here, N_q is the number of quantum nuclei of mass m_q, N_p is the number of encapsulating point-like nuclei, $\hat{V}_{qp}$ is a quantum point-like nuclei potential energy operator and $\hat{V}_{qq}$ is a quantum-quantum nuclei potential energy operator. We use atomic units through this document. In this section, we employ lowercase i, j as quantum nuclei indices and uppercase I as point-like nuclei index.

The wavefunction for identical fermionic nuclei in the HF representation is expressed as a single Slater determinant, which is an antisymmetrized product of spin-orbitals [62]

$$|\,\Psi_{\mathrm{HF}}\rangle = |\prod_{i}^{N_q} \chi_i\rangle. \tag{2}$$

Here, each spin-orbital χ_i is the product of an orbital ψ_i and a nuclear spin function. For a nuclear spin s, there are $2s+1$ orthonormal spin functions. Orbitals, ψ, are constructed as linear combinations of basis functions, and their combination coefficients are obtained by solving the one-particle Fock equations, $\hat{f}\psi_i = \varepsilon_i \psi_i$.

In the NC-NOCI approach, the wavefunction

$$\mid \Psi_{\mathrm{NOCI}}\rangle = \sum_{A}^{N_{conf}} C_A \mid \Psi_A\rangle, \tag{3}$$

is expressed as a linear combination of N_{conf} Hartree-Fock wavefunctions Ψ_A. Here, we use indices A and B as configuration iterators.

The energy diagonal matrix, $\mathbf{E}$, and combination coefficients matrix, $\mathbf{C}$, are determined by solving the NC-NOCI matrix equation

$$\mathbf{H}^{\mathrm{NO}}\mathbf{C} = \mathbf{S}^{\mathrm{NO}}\mathbf{C}\mathbf{E}. \tag{4}$$

The elements of the NC-NOCI overlap, $\mathbf{S}^{\mathrm{NO}}$, and Hamiltonian matrices, $\mathbf{H}^{\mathrm{NO}}$, are evaluated following the method of Ref.[63]. An element S^{NO}_{AB} of $\mathbf{S}^{\mathrm{NO}}$ is computed as the determinant of the occupied orbitals overlap,

$$S^{\mathrm{NO}}_{AB} = \langle \Psi_A | \Psi_B \rangle = |\mathbf{S}|. \tag{5}$$

Here, $\mathbf{S}$ is the overlap matrix between occupied orbitals that belong to configurations A and B. The elements, S_{ij}, of this matrix are of the form

$$S_{ij} = \langle \psi_{i\in A} | \psi_{j\in B} \rangle. \tag{6}$$

The computed S^{NO}_{AB} terms are used to evaluate the elements, H^{NO}_{AB}, of $\mathbf{H}^{\mathrm{NO}}$, as

$$\begin{aligned} H^{\mathrm{NO}}_{AB} &= \langle \Psi_A | \hat{H} | \Psi_B \rangle \\ &= S^{\mathrm{NO}}_{AB}\Bigg(\sum_{i\in A}^{N_q}\sum_{j\in B}^{N_q} \langle \psi_i | \hat{h}_q | \psi_j \rangle S^{-1}_{ji} \\ &+ \frac{1}{2}\sum_{ii'\in A}^{N_q}\sum_{jj'\in B}^{N_q} \langle \psi_i \psi_{i'} | \hat{V}_{qq} | \psi_j \psi_{j'} \rangle [S^{-1}_{ji} S^{-1}_{j'i'} - S^{-1}_{j'i} S^{-1}_{ji'}] \Bigg), \end{aligned} \tag{7}$$

where S^{-1}_{ji} is an element of the occupied orbitals inverse matrix $\mathbf{S}^{-1}$. Here, the core operator, $\hat{h}_q$, is

$$\hat{h}_q(\mathbf{r}) = -\frac{\nabla^2_r}{2m_q} + \sum_{I}^{N_p} \hat{V}_{qI}(\mathbf{r} - \mathbf{R}_I). \tag{8}$$

Once the generalized eigenvalue problem is solved, the density matrices of the NC-NOCI states can be expressed in terms of the atomic orbital basis set employed in the NC-HF calculations. In this study, we propose employing the NC-NOCI approach to characterize the $He_2@C_{60}$ system.

$He_2@C_{60}$ effective potentials

We derive the nuclear Hamiltonian for the $He_2@C_{60}$ system from the general Hamiltonian in Eq. 1

$$\hat{H}^{\mathrm{He}} = -\sum_{i}^{2} \frac{\nabla^2_i}{2m_{\mathrm{He}}} + \sum_{i}^{2} \hat{V}_{\mathrm{He-C_{60}}}(\mathbf{r}_i) + \hat{V}_{\mathrm{He-He}}(\mathbf{r}_{12}). \tag{9}$$

Here, $\hat{V}_{\mathrm{He-C_{60}}}$ represents the effective interaction potential between each He and the C_{60} walls, and $\hat{V}_{\mathrm{He-He}}$ denotes the He–He effective interaction potential.

To obtain the $\hat{V}_{\mathrm{He-He}}$ potential, calculations were performed at the CCSD(T)/aug-cc-pVnZ ($n = 3-5$) level combined with the complete basis set (CBS) extrapolation technique[64]. Various He–He internuclear distances $\mathbf{r}_{12}$ were considered. The effective potential was determined by calculating the energy difference between the He dimer and two free He atoms, $V_{\mathrm{He-He}}(\mathbf{r}_{12}) = E_{\mathrm{He-He}}(\mathbf{r}_{12}) - 2E_{\mathrm{He}}$. To simplify the calculation of matrix elements in the open-LOWDIN code[65], the potential function was expanded using Gaussian type functions (GTFs)

$$\hat{V}_{\mathrm{He-He}}(\mathbf{r}_{12}) = \sum_{l}^{N} c_l \exp(-\alpha_l \mathbf{r}^2_{12}) \tag{10}$$

The expansion coefficients, c_l, and exponents, α_l, of the GTFs are provided in Table S.3 in the SI. Figure S.2 in the SI compares the fitted potentials and the CCSD(T) interaction energies.

Using the GTF expansion of $\hat{V}_{\mathrm{He-He}}$, the elements of the NC-HF two-particle matrix are calculated from four-center integrals of the form

$$\left\langle \mu\sigma \mid \hat{V}_{\mathrm{He-He}} \mid \nu\lambda \right\rangle = \sum_{l}^{N} c_l \left\langle \mu\sigma \mid \exp(-\alpha_l \mathbf{r}^2_{12}) \mid \nu\lambda \right\rangle, \tag{11}$$

where $\mu, \nu, \sigma, \lambda$ are GTF basis functions, and we employed the physicist's notation for the four-center integrals[62]. These integrals are evaluated using the contracted Gaussian Geminal operator implemented in the latest version of the Libint library[66].

To construct the $\hat{V}_{\mathrm{He-C_{60}}}$ potential, we followed several steps. First, the geometry of C_{60} was optimized at the B3LYPD3/def2-SVP level of theory, imposing the I_h point group. This optimized geometry was kept fixed in subsequent calculations. Next, MP2/cc-pVDZ level energy calculations were performed for a system comprising a He atom inserted into C_{60}. In these calculations, the He atom was gradually displaced along a line connecting the center of mass of C_{60} (CM) and the center of a hexagon face of the cage. At each displacement point, the interaction energy was computed as $V_{\mathrm{He-C_{60}}}(\mathbf{r}) = E_{\mathrm{He@C_{60}}}(\mathbf{r}) - E_{\mathrm{C_{60}}} - E_{\mathrm{He}}$. These interaction energies were then fitted to a sum of Lennard-Jones (8-6) potential terms for each helium-carbon pair distance ($r = |\mathbf{r} - \mathbf{R}_j|$) in C_{60}, represented as $V_{\mathrm{He-C}}(r) = A/r^8 - B/r^6$. The fitting procedure allowed us to determine the attractive ($A = 604.05\ E_h a_0^8$), and repulsive ($B = 17.17\ E_h a_0^6$) parameters.

To facilitate the evaluation of matrix elements in terms of a Gaussian basis set, the Lennard-Jones function was expressed as a linear combination of N Gaussian functions. The total $\hat{V}_{\mathrm{He-C_{60}}}$ potential employed was of the form

$$\hat{V}_{\mathrm{He-C_{60}}}(\mathbf{r}) = \sum_{I}^{60}\sum_{l}^{N} c_l \exp(-\alpha_l(\mathbf{r} - \mathbf{R}_I)^2). \tag{12}$$

The expansion coefficients, c_l, and exponents, α_l, are provided in Table S.4 along with the C_{60} coordinates ($\mathbf{R}_I$) in Table S.1 in the SI. Figure S.1 in the SI compares the fitted potentials and the MP2 interaction energies. By employing the GTF expansion of $\hat{V}_{\mathrm{He-C_{60}}}$, the matrix elements of the NC-HF one-particle potential matrix are easily calculated from three-center overlap integrals,

$$\left\langle \mu \mid \hat{V}_{\mathrm{He-C_{60}}} \mid \nu \right\rangle = \sum_{I}^{60}\sum_{l}^{N} c_l \left\langle \mu \mid \exp(-\alpha_l(\mathbf{r} - \mathbf{R}_I)^2) \mid \nu \right\rangle. \tag{13}$$

For reference, we utilized the combined quantum harmonic oscillator and rigid rotor (HO+RR) approximations to solve the nuclear Schrödinger equation of $He_2@C_{60}$. To obtain comparable results to the NC-HF and NC-NOCI energies, we considered only the six degrees of freedom of He_2 with the Hamiltonian of Eq. 9. To find the frequencies of the harmonic oscillator modes, we computed the hessian matrix at the minimum of the potential energy along a C_3 symmetry axis, ($r = \pm 1.829$ a_0). Four normal modes were considered as harmonic, three translations, with frequencies of 167, 167, and 298 cm^{-1}, and one stretching, with frequency of 582 cm^{-1}. The coordinates of these modes are provided in Table S.2 in the SI. The two remaining modes were considered rotations. The rigid rotor energy states were computed assuming a He_2 pseudo-molecule with bond length $r = 3.658$ a_0 and rotational constant $B = 2.967$ cm^{-1}.

In this simplified HO+RR model, the energy is calculated as the sum of the potential energy minimum (V_{min}) with the energy of the harmonic and rotational modes. Notably, the rotational energy, $E_{rot} = 2BJ(J+1)$, of the ground state ($J = 0$) is zero.

Representation of the $He_2@C_{60}$ HF wavefunction

At the HF level, helium orbitals are constructed as linear combinations of a set of basis GTFs in two alternative ways. In the first, the basis set is centered at the CM of C_{60}, inspired by the nearly spherical symmetry of C_{60}. Here, we employed 13 s-type and 13 p-type GTFs, with even-tempered exponents ranging from 10.0 to 0.10 a_0^{-2}.

In the second way, the basis set is centered on two centers (TC) symmetrically separated from the CM along a C_3 symmetry axis. This choice is inspired by electronic structure geometry optimization results reporting that the He−He separation inside C_{60} is around 3.7 a_0 and energy differences between orientations along any of the symmetry axis are negligible ($< 10^{-4}$ E_h)[32].

To select the optimal TC basis parameters, we followed several steps. First, we placed two [1s] GTFs and minimized the energy with respect to their separation and exponent. Then, at this optimized position (r=±1.851 a_0), we performed calculations employing [1s1p], [1s1p1d] or [1s1p1d1f] basis sets. The exponents of these GTFs were also optimized and are presented in Table 1.

Table 1. Optimized He basis set exponents (a_0^{-2}) for NC-HF calculations in the two-center basis set approach (r=±1.851 a_0).

l	[1s]	[1s1p]	[1s1p1d]	[1s1p1d1f]
s	3.8187	3.8373	4.8697	4.9789
p		3.8185	2.6936	2.5311
d			3.4703	3.3983
f				3.2064

Procedure to generate the NC-NOCI configurations

To generate configurations, NC-HF calculations were performed using TC basis sets located at various positions. In view of the nearly spherical symmetry of C_{60} we selected the He basis set positions from Lebedev angular grids[67], with 110, 192, and 302 points, in a radius $r = 1.851$ a_0, corresponding to the optimized HF center positions obtained from the previous step.

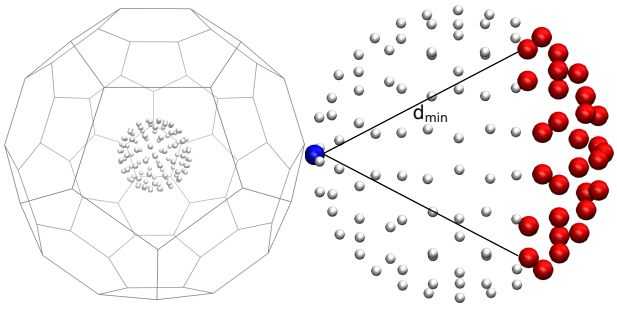

Figure 1. Schematic representation of the multicenter basis placement used in NC-NOCI calculations. From a Lebedev grid (in white) we select one point to position the first set of basis functions (shown in blue). Next, we select a second point at a minimum distance of d_{min} to place the second basis set (indicated in red). NC-HF calculations are performed for every combination of these points.

We propose a geometric criterion to reduce the number of configurations in the NC-NOCI expansion: a configuration is included only if the distance between its basis set centers d is $d_{min} < d < 2r$, where d_{min} is a cutoff and $2r$ is the maximum distance between points in the Lebedev grid. Figure 1 illustrates a schematic representation of the nearly spherical grid, showcasing the possible basis set combinations at a given d_{min} value. The results of NC-NOCI calculations with different d_{min} values were contrasted with NC-FCI outcomes obtained using the 110 grid of [1s] basis functions. In subsection NC-NOCI energies we discuss the choice of an optimal d_{min} value.

In NC-HF calculations, self-consistent field (SCF) convergence was achieved when the change in energy between two successive iterations reached a value lower than 10^{-10} E_h. In NC-NOCI calculations, Hamiltonian matrix elements are assigned a value of zero when the overlap of the corresponding configurations is lower than 10^{-8}.

The NC-HF and NC-NOCI methods were implemented in the openLOWDIN package[65], which is an open version branch of the LOWDIN software[68]. The current implementation of the NC-HF and NC-NOCI supports multiple types of quantum particles following the Any Particle Molecular Orbital framework[69]. All electronic structure calculations were carried out using the ORCA 5.0.3 package[70]. Orbital and density plots were generated with the VMD software[71].

Results and Discussion

NC-HF analysis

We conducted several NC-HF calculations for o−$He_2@C_{60}$ and p-$He_2@C_{60}$ configurations employing CM and TC basis set centers. The orbitals obtained employing the CM basis set are labeled according to the irreducible representations of the I_h group. On the other hand, the axis selection in the TC approach lowers the symmetry of the system from I_h to D_{2h}. Here, He_2 may be viewed as a linear molecule with an inversion center. Therefore, we use the $\sigma_{g/u}$ notation to refer to the TC orbitals.

Table 2. $He_2@C_{60}$ NC-HF energy components (mE_h) for *o*-$He_2@C_{60}$ ($^3\Psi$) and *p*-$He_2@C_{60}$ ($^1\Psi$) configurations. The sum of the potential energy minimum (V_{min}) with the simplified HO+RR energy is presented for reference[a]

Configuration	Basis	Center/a_0	E_{total}	$\langle K_{He}\rangle$	$\langle V_{He-He}\rangle$	$\langle V_{He-C_{60}}\rangle$
$^1\Psi = \|a_g^2\rangle$	[13s]	0	134.729	0.843	94.122	39.764
$^1\Psi = \|\sigma_g^2\rangle$	[1s]	± 1.851	1841.632	2.085	1836.274	3.273
$^3\Psi = \|1a_g 2a_g\rangle$	[13s]	0	48.426	1.990	29.003	17.433
$^3\Psi = \|a_g t_{1u}\rangle$	[13s13p]	0	35.458	0.681	21.511	13.266
$^3\Psi = \|\sigma_g\sigma_u\rangle$	[1s]	± 1.851	8.213	2.085	2.855	3.273
	[1s1p]		8.213	2.081	2.823	3.308
	[1s1p1d]		7.667	1.792	2.619	3.256
	[1s1p1d1f]		7.634	1.765	2.787	3.082
V_{min}+ HO+RR	-	± 1.829	6.961	1.377		

[a] Two-center calculations were performed placing the basis sets along a C_3 axis. $V_{min} = 4.207$ was also computed along a C_3 axis.

Table 2 presents the NC-HF energies obtained for $o-He_2@C_{60}$ *o*-$He_2@C_{60}$. a_g and t_{1u} orbitals obtained with the CM basis set are more delocalized than σ_g and σ_u orbitals obtained with the TC basis set. The higher delocalization displayed by the CM orbitals indicates that the He atoms get closer to the walls of the C_{60}, thereby increasing their repulsion. Furthermore, the delocalized orbitals display a higher overlap, which in turn generates a higher He-He repulsion.

The NC-HF calculations are utilized as a reference for identifying the optimal size and centers of the basis set. The convergence of CM and TC calculations should yield equivalent energies upon reaching the complete basis set limit. Although we have not reached this limit, the NC-HF results obtained with a single-determinant wavefunction clearly predict a localized triplet ground state. The remaining calculations in this paper only consider the TC basis sets.

When describing two helium atoms enclosed within C_{60} using TC orbitals, one approach to obtain physically meaningful energies for *p*-$He_2@C_{60}$ is to generate a spin-adapted configuration as a linear combination of two open-shell determinants[62]. At the optimized distance of the TC basis sets, the overlap between these functions is negligible, resulting in minimal contribution from exchange integrals. Therefore, an open-shell wavefunction, $\Psi = |\sigma_g^\alpha \sigma_u^\beta\rangle$, yields the same energy as the corresponding $^3\Psi$ state presented in Table 2. However, the reduced overlap also leads to the maximum possible spin contamination[62]. This spin contamination is removed by employing a spin-adapted configuration, $^1\Psi = |\sigma_g^\alpha \sigma_u^\beta\rangle - |\sigma_g^\beta \sigma_u^\alpha\rangle$. Spin-adapted configurations are explicitly considered within the NC-NOCI method by generating two open-shell singlet HF wavefunctions for each He−He TC orientation.

For *p*-$He_2@C_{60}$ with the CM basis, we obtained a $|a_g{}^2\rangle$ ground state configuration with total energy 135 mE_h. With the TC basis, we obtained a $|\sigma_g^2\rangle$ configuration with a total energy of 1842 mE_h. Regardless of the choice of basis set centers, the calculated NC-HF energies for low-spin nuclear configurations are unphysically large compared to reference values from the simplified HO+RR model.

Unusual high energies have also been observed in HF calculations involving low-spin configurations of identical fermionic nuclei, such as of doped He_2 singlet systems[49], and the two ^1H nuclei in H_2[72]. These high-energy outcomes are attributed to the limitations of single-configurational wavefunctions in describing singlet states. This is primarily due to the presence of large spurious self-repulsion integrals. In regular electronic calculations, these self-repulsion integrals also become problematic when describing the dissociation of a closed-shell molecule into open-shell fragments. For example, the dissociation of the H_2 molecule is not correctly described at the restricted HF level because the energy includes a one-center electron-electron repulsion integral unbalanced at larger distances[62].

On the other hand, self-repulsion integrals are absent from the HF energies of high-spin configurations[62,72]. As a consequence, the ground state energies of *o*-$He_2@C_{60}$ presented in Table 2 are considerably lower than those of *p*-$He_2@C_{60}$, irrespective of the basis set size and center. For the CM basis, the total energy of *o*-$He_2@C_{60}$ obtained with [13s] GTFs 48.426 mE_h, is reduced to 35.458 mE_h when the basis is expanded to [13s13p] GTFs. These results are still considerably higher compared to the simplified HO+RR model one of 6.961 mE_h.

The TC basis set results for *o*-$He_2@C_{60}$ also show a gradual decrease in total energy as the number of basis functions with different angular momentum increases. Similar total energies are predicted with the [1s1p1d] and [1s1p1d1f] basis sets, 7.667 mE_h and 7.634 mE_h, respectively. These total energies are lower than those of the CM basis set and are comparable to that of the simplified HO+RR model. Further inspection of Table 2 reveals that the potential energy terms $\langle V_{He-He}\rangle$ and $\langle V_{He-C_{60}}\rangle$ are one order of magnitude larger for the CM basis results than for the TC basis results.

To gain insight on the potential energy difference between CM and TC results, Figure 2 depicts NC-HF orbitals for

NC-NOCI energies

To initiate the NC-NOCI calculations, it is essential to determine the optimal value for the cutoff distance (d_{min}) between the TC basis functions. Figure 3 illustrates the variation in total NC-NOCI energies as a function of d_{min}, using [1s] basis sets distributed across a 110-point grid. Additionally, it includes NC-FCI results obtained using the same basis set. The figure reveals that reducing d_{min} increases the number of NC-HF configurations included in the NC-NOCI expansion, resulting in the total energies converging towards the NC-FCI results. It also indicates that the singlet and triplet state energies converge at a similar rate as d_{min} decreases. Consequently, the NC-NOCI *o*-*p* splitting

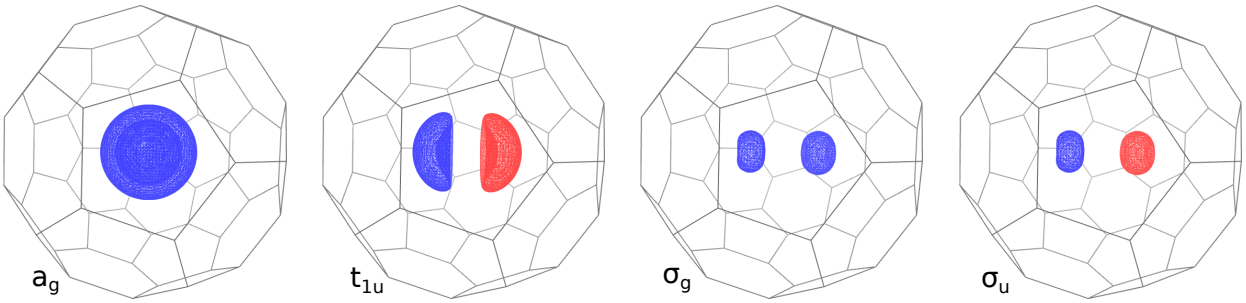

Figure 2. NC-HF orbitals for $He_2@C_{60}$ in triplet configurations. CM orbitals, a_g and t_{1u}, were obtained with a 13s13p even-tempered basis set. TC orbitals, σ_g and σ_u, were obtained with optimized [1s1p1d] basis functions centered at ± 1.851 a_0. Contour values: ± 0.1 $a_0^{-3/2}$

achieves convergence with a smaller number of configurations compared to total energies.

Choosing the right value for d_{min} is crucial in NC-NOCI calculations. A smaller value brings the energy closer to the variational limit but significantly increases the computational cost, which scales quadratically with the number of configurations. The creation of the Hamiltonian matrix ($\mathbf{H}^{\mathrm{NO}}$) is a bottleneck for NC-NOCI calculations.

In our calculations, we chose $d_{min} = 3.6$ a_0, as shown in Figure 3. This selection ensures that the NC-NOCI energy is only 5×10^{-6} E_h higher than the FCI energy. Importantly, with this d_{min} value, the NC-NOCI splitting closely approximates the FCI prediction, differing by only 0.002 cm^{-1}. This choice of d_{min} incorporates 758 configurations in the NC-NOCI expansion, accounting for only 6% of the total FCI configurations.

Table 3 presents the energies for p-$He_2@C_{60}$ and o-$He_2@C_{60}$ obtained with NC-NOCI and different combinations of grids and basis set sizes. As anticipated from the variational nature of the NC-NOCI method, the energies decrease as the number of basis set functions and grid points increase. Notably, increasing the number of basis functions yields a more significant reduction in energy compared to increasing the number of grid points. In contrast to NC-HF, the NC-NOCI method predicts that o-$He_2@C_{60}$ has higher energy than p-$He_2@C_{60}$. The NC-NOCI method predicts o-p energy splitting of 5.69 cm^{-1} with the basis+grid combination that leads to the lowest energies, [1s1p1d] GTFs in 194 points.

As reference values, Table 3 also displays the p-$He_2@C_{60}$ and o-$He_2@C_{60}$ energies and o-p splitting predicted by the simplified HO+RR model.

To compute these energies, we consider the symmetry of the spatial and spin wavefunctions. The ground state functions of the harmonic oscillator and rigid rotor ($J = 0$) are symmetric, so the antisymmetry of the nuclear wavefunction is determined by the spin function of p-$H_2@C_{60}$ (nuclear spin $S = 0$). The first nuclear-excited state consists of the ground state harmonic oscillator functions combined with the $J = 1$ state of the rigid rotor. Since the $J = 1$ rotational wavefunction is antisymmetric, the antisymmetry of the nuclear wavefunction is preserved with a symmetric o-$H_2@C_{60}$ spin state ($S = 1$). Therefore, the energy of this first excited state differs from the ground state by the rotational energy of the rigid rotor $J = 1$ ($2B$).

Consistent with the results of the simplified HO+RR model, our NC-NOCI analysis successfully predicts the correct spin symmetry of the ground nuclear state of $He_2@C_{60}$ and its o-p splitting energy. The lowest NC-NOCI energies and the simplified HO+RR model results exhibit a difference of only 0.29 mE_h (4%) for both p-He_2 and o-He_2 states. Likewise, the o-p splitting prediction differs by only 0.24 cm^{-1} between the two approaches.

The agreement between the predictions of both models strongly suggests that the NC-NOCI approach captures the correct physical description of the system. However, at this stage, we are unable to confirm which prediction is more accurate. In the framework of the effective potentials we are utilizing, the accuracy in the calculation of total nuclear energy considering the simplified HO+RR model is impacted by the validity of the decoupling of the translational, rotational, and vibrational degrees of freedom. Furthermore, this model omits the contribution of anharmonic potential energy terms. In contrast, the accuracy of the NC-NOCI approach is impacted by the basis set incompleteness error. In addition, the NC-NOCI results converge to the NC-FCI only for [1s] basis sets. For larger basis sets, the NC-NOCI energies will converge to a higher value than the corresponding NC-FCI energy because the current NC-NOCI approach only mixes ground state NC-HF determinants.

NC-NOCI densities

Figure 4 displays the NC-NOCI ground state density of p-$He_2@C_{60}$. The panel with the highest contour value (0.088 a_0^{-3}) exhibits 20 density maxima. These maxima form an icosahedron, with their vertices pointing towards the hexagon faces of C_{60}. This is evidence of how the NC-NOCI wavefunction responds to the anisotropy of the $V^{\mathrm{He-C_{60}}}$ potential, indicating the orientations with the highest likelihood of finding He atoms. However, as the contour values slightly decrease (0.06 a_0^{-3}), the other panels in Figure 4 demonstrate that the probability density becomes nearly spherical. Consequently, the probability of finding the He-He pseudo-molecule in any other direction within the system is significant. These results indicate that the He dimer has nearly free rotations inside the C_{60} even at 0 K.

Figure 5 presents the NC-NOCI density for the lowest-energy triply degenerate o-$He_2@C_{60}$ states. The displayed densities correspond to spatial wavefunctions of T_{1u} symmetry. The three o-He_2 states exhibit equivalent density distributions, each with two maxima along a preferred C_2 symmetry axis. These preferred axes pass through C=C (6-6) bonds of C_{60} and have 90° angles between them. Assuming that these three degenerate states are in a superposition with equal probabilities, the resulting density becomes icosahedral, with 20 equivalent maxima symmetrically located along the 10 C_3 rotation axis of C_{60}, as shown in the

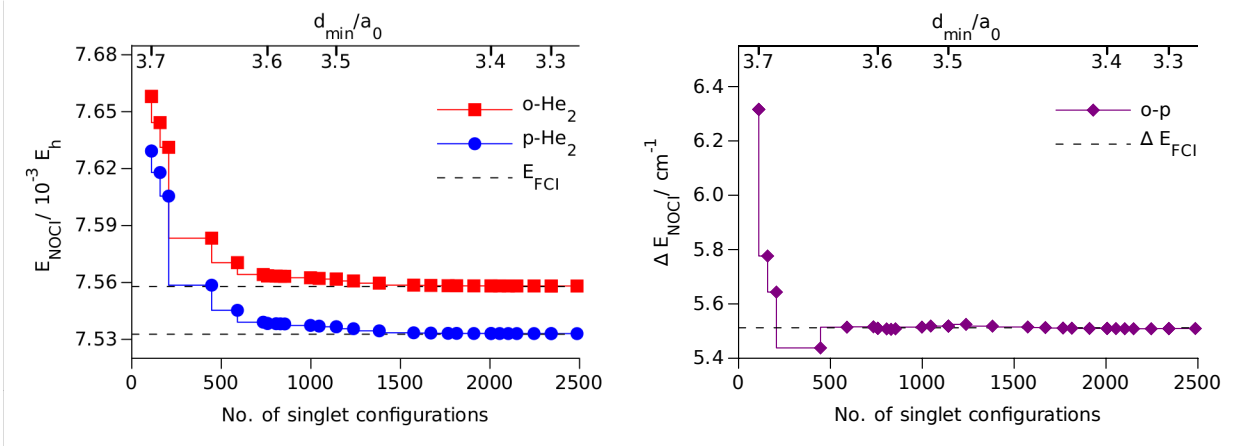

Figure 3. NC-NOCI ground state energy for the singlet and triplet states of $He_2@C_{60}$ (left) and their difference (right) as a function of the number of HF configurations included in the CI expansion. The number of configurations is determined by the minimum separation between He basis functions, d_{min}. The number of triplet configurations mixed is half the number of singlet configurations. Calculations were performed with [1s] basis sets on the 110-point Lebedev grid with $r = 1.851$ a_0. FCI results with the same basis set (12100 configurations) are presented for reference.

Table 3. NC-NOCI and NC-FCI ground state energies (in mE_h) for the singlet and triplet states of $He_2@C_{60}$ computed with different basis sets and Lebedev grids. All Lebedev grids use $r = 1.851$ a_0, and all NC-NOCI calculations were performed with $d_{min} = 3.6$ a_0. For reference, the harmonic oscillator and rigid rotor model results are also presented.

Method	Basis	No. centers	No. Conf.[a]	$E(p\text{-He}_2)/10^{-3}E_h$	$E(o\text{-He}_2)/10^{-3}E_h$	$\Delta E/cm^{-1}$
FCI	[1s]	110	12100	7.533	7.558	5.51
	[1s]	194	37636	7.527	7.551	5.34
NOCI	[1s]	110	758	7.538	7.563	5.51
	[1s]	194	1850	7.528	7.552	5.34
	[1s]	302	5462	7.527	7.552	5.34
	[1s1p]	110	758	7.520	7.543	5.15
	[1s1p]	194	1850	7.502	7.525	5.05
	[1s1p1d]	110	758	7.261	7.288	5.79
	[1s1p1d]	194	1850	7.253	7.279	5.69
HO+RR	-	-	-	6.961	6.988	5.93

[a] The number of triplet configurations mixed in the NC-NOCI expansion is half that of the singlet.

bottom panel of Figure 5.

The nearly spherical densities shown in 4 and Figure 5 offer insights into the similarities between the NC-NOCI and the simplified HO+RR model results. In the quantum rigid rotor model, the solutions are represented using spherical harmonics. For $J = 0$, the solution is a constant, indicating that every orientation has the same probability. Similarly, assuming that the three degenerate functions with $J = 1$ are in a superposition with equal probability, we obtain a radially symmetric density distribution.

The energies obtained from the HO+RR and NC-NOCI approaches show remarkable agreement. This is also consistent with the similarity between the spherical densities predicted with HO-RR and the nearly spherical densities observed in the NC-NOCI. However, the NC-NOCI method provides a more comprehensive description of the density distributions, as it correctly responds to the icosahedral symmetry of the external potential.

Finally, Figure 6 presents an energy diagram summarizing the NC-NOCI and simplified HO+RR predictions for the first $He_2@C_{60}$ excited states. The first NC-NOCI p-He_2 excited states are five-fold degenerate, with a relative energy only 0.62 cm^{-1} lower than the HO-RR states with $J = 2$. In contrast, the first excited state of o-He_2 does not exhibit the seven-fold degeneracy of $J = 3$. Instead, there are four degenerate states 3.7 cm^{-1} below $J = 3$ and three degenerate states 2.4 cm^{-1} above $J = 3$. A similar result is observed for the second p-He_2 excited state, where four states are 4.4 cm^{-1} below $J = 4$ and five 0.9 cm^{-1} above $J = 4$.

It is well known that external fields break the degeneracy of the spherical harmonics according to the symmetry of the potential[73,74].

Inspecting the character table of the I_h group[74], we observe that all the spherical harmonics with $J = 1$ and $J = 2$ belong to irreducible representations T_{1u} and H_g respectively. Therefore, the degeneracy of these states is not lifted by an external I_h potential. On the other hand, for $J = 3$ three states have G_u and four have T_{2u} symmetries. Likewise, for $J = 4$ four states have G_g and five have H_g symmetries. As a consequence, an external I_h potential, will lift the degeneracy between $J = 3$ G_u and T_{2u} states and between $J = 4$ G_g and H_g states.

Considering these factors, the expected degeneracy pattern for the spherical harmonics in an external I_h potential matches perfectly the degeneracy observed in the NC-NOCI excited states. Therefore, these results provide further evidence that the NC-NOCI method correctly describes the response of the nuclear wavefunction to the symmetry of the external potential.

Conclusions

We have conducted a study on the energies and structure of two ^{3}He atoms trapped in C_{60}, utilizing a Hamiltonian that draws parallels between endohedral systems and many-electron atoms. In this Hamiltonian, the interactions of the trapped particles are represented by effective NC potentials. When employing the HF method to obtain He wavefunctions, our results demonstrate that spin and spatial symmetries are broken to lower the energy. To ensure wavefunctions with the correct symmetries, we employed a NC-NOCI method, which mixes the broken-symmetry HF wavefunctions.

For the p-He_2 system, our NC-NOCI predicts a ground state that displays an A_g singlet configuration. For o-He_2, the ground state is triply degenerate with T_{1u} symmetry, and is 5.69 cm^{-1} higher in energy compared to p-He_2. These observations align perfectly with the expected symmetries and energies obtained with a simplified HO+RR model, which predicts a 5.93 cm^{-1} o-p energy difference. Furthermore, the NC-NOCI nuclear densities obtained for p-He_2 and o-He_2 display the icosahedral symmetry of the C_{60} embedding potential. In addition, the energies of the first NC-NOCI excited states display the expected splitting pattern derived from a symmetry analysis of the spherical harmonics interacting with an external icosahedral field.

To the best of our knowledge, this is the first theoretical study that highlights the relevance of the fermionic nature of ^{3}He nuclei in describing confined He atoms within fullerenes. Given that $He_2@C_{60}$ has been detected[26] and synthesized[27], it may be feasible to experimentally determine the $o - p$ splitting in $^3He_2@C_{60}$.

In future research, we plan to investigate endohedral systems with three or more He nuclei to explore the possible formation of nuclear shells, similar to what is observed in the electronic structure of atoms. We will also perform calculations on other fullerenes holding two He atoms[75], to analyze the impact of different encapsulating symmetries on the $o - p$ splitting.

It is important to note that while the proposed method may not be as accurate as other approaches used to describe the quantum nature of endohedral atoms and molecules[76], such as FCI[54] and multiconfigurational time-dependent Hartree[77] approaches, it offers generality.

The NC Hamiltonian employed, and the NC-NOCI implementation in the openLOWDIN code is not limited to the system studied in this manuscript. Instead, it can be applied to describe any embedded system with any number of particles, where the interactions can be physically represented through pair-wise potentials. Thus, the proposed approach can be used to investigate nuclear quantum effects of a variety of confined species affected by effective isotropic or anisotropic potentials. Of particular interest to us is the application of this methodology to analyze the energy splitting of p-H_2O and o-H_2O in different chemical environments.

Acknowledgements

FM and LGMP acknowledge financial support from the European Research Council (ERC) Advanced Grant under Project No. 101021166 - GAS-WAT. The Swedish National Infrastructure for Computing (SNIC) is acknowledged for providing computational resources at the High-Performance Computing Center North (HPC2N). AR acknowledges the financial support of the Office of Research of the National University of Colombia (QUIPU codes: 400000035813, 201010040226) WQ acknowledges the financial support of the ANID/Doctorado Nacional/21222021 Ph.D. fellowship.

Conflict of Interest

The authors declare no conflict of interest.

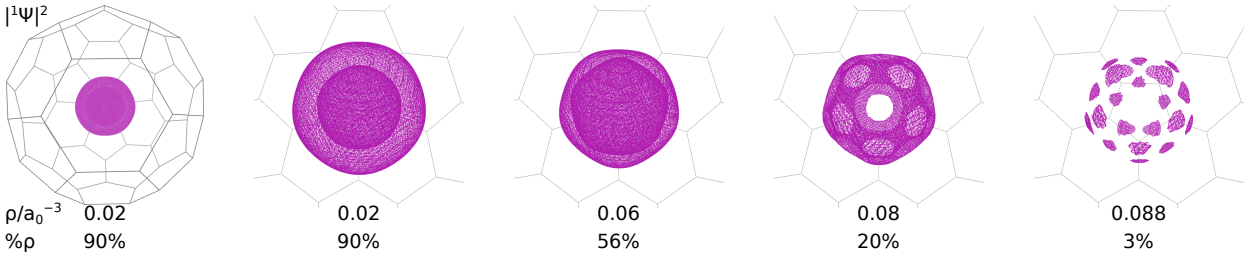

Figure 4. Density contours for the lowest energy NC-NOCI singlet state of $He_2@C_{60}$. NC-NOCI calculations obtained from 194 possible He positions with the [1s1p1d] basis set.

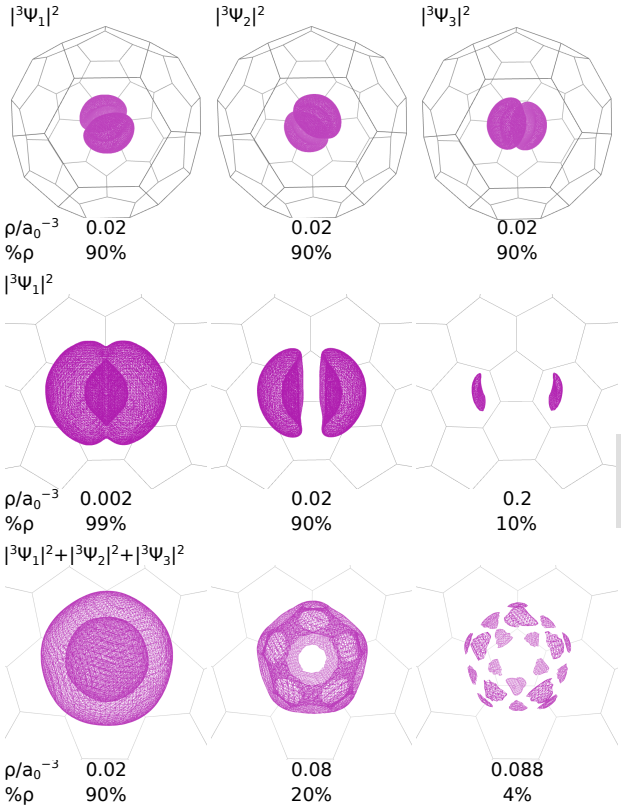

Figure 5. Density contours for the lowest energy NC-NOCI triplet states of $He_2@C_{60}$ (top). Selected contour values for one triplet state (middle). Selected contour values for the average of the three triplet densities (bottom). NC-NOCI calculations obtained from 194 possible He positions with the [1s1p1d] basis set.

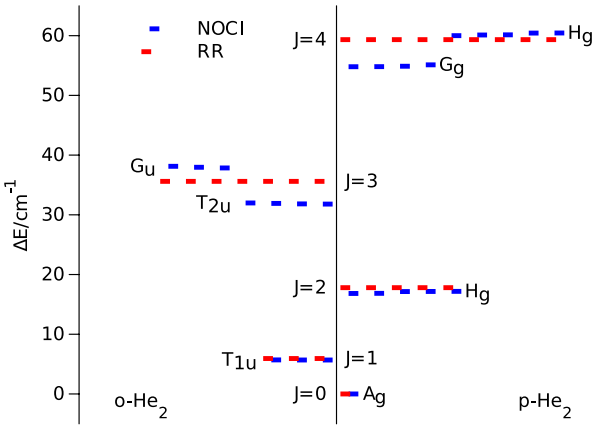

Figure 6. Relative energy diagram for the 32 first NC-NOCI and RR states of $He_2@C_{60}$. Energy differences with respect to the NC-NOCI (7.253 mE_h) and HO-RR (6.961 mE_h) *p*-$He_2@C_{60}$ ground-state. The NC-NOCI states are classified according to their irreducible representations. NC-NOCI calculations obtained from 194 possible He positions with the [1s1p1d] basis set.

Keywords: Nuclear quantum effects • Ab-initio calculations • Confined atoms • Endohedral fullerenes • Nuclear spin effects

References

[1] T. Miyazaki, *Atom tunneling phenomena in physics, chemistry and biology*, volume 36, Springer Science & Business Media **2004**.

[2] M. Wolfsberg, W. Van Hook, P. Paneth, L. Rebelo, *Isotope Effects: in the Chemical, Geological, and Bio Sciences*, Springer Netherlands **2009**.

[3] J. Kästner, S. Kozuch, *Tunnelling in Molecules: Nuclear Quantum Effects from Bio to Physical Chemistry*, ISSN, Royal Society of Chemistry **2020**.

[4] T. Ishimoto, M. Tachikawa, U. Nagashima, *Int. J. Quantum Chem.* **2009**, *109*, 2677.

[5] N. F. Aguirre, P. Villarreal, G. Delgado-Barrio, E. Posada, A. Reyes, M. Biczysko, A. O. Mitrushchenkov, M. P. de Lara-Castells, *J. Chem. Phys.* **2013**, *138*.

[6] M. Ceriotti, W. Fang, P. G. Kusalik, R. H. McKenzie, A. Michaelides, M. A. Morales, T. E. Markland, *Chem. Rev.* **2016**, *116*, 7529.

[7] T. E. Markland, M. Ceriotti, *Nat. Rev. Chem.* **2018**, *2*.

[8] F. Pavošević, T. Culpitt, S. Hammes-Schiffer, *Chem. Rev.* **2020**, *120*, 4222.

[9] G. Cassone, *J. Phys. Chem. Lett.* **2020**, *11*, 8983.

[10] A. Kundu, Y. Song, G. Galli, *Proc. Natl. Acad. Sci. U.S.A.* **2022**, *119*, e2203083119.

[11] N. J. Turro, *Proc. Natl. Acad. Sci. U.S.A.* **1983**, *80*, 609.

[12] E. A. Chekhovich, M. N. Makhonin, A. I. Tartakovskii, A. Yacoby, H. Bluhm, K. C. Nowack, L. M. K. Vandersypen, *Nat. Mater.* **2013**, *12*, 494.

[13] J. B. Lambert, E. P. Mazzola, C. D. Ridge, *Nuclear Magnetic Resonance Spectroscopy: An Introduction to Principles, Applications, and Experimental Methods*, Wiley **2019**.

[14] A. Schweiger, G. Jeschke, *Principles of Pulse Electron Paramagnetic Resonance*, Oxford University Press **2001**.

[15] C. Puzzarini, J. F. Stanton, J. Gauss, *Int. Rev. Phys. Chem.* **2010**, *29*, 273.

[16] U. Ranieri, M. M. Koza, W. F. Kuhs, R. Gaal, S. Klotz, A. Falenty, D. Wallacher, J. Ollivier, P. Gillet, L. E. Bove, *J. Chem. Phys. C.* **2019**, *123*, 1888.

[17] J. Tennyson, P. F. Bernath, L. R. Brown, A. Campargue, A. G. Császár, L. Daumont, R. R. Gamache, J. T. Hodges, O. V. Naumenko, O. L. Polyansky, Others, *J. Quant. Spectrosc. Radiat. Transf.* **2013**, *117*, 29.

[18] P. Villarreal, M. de Lara-Castells, R. Prosmiti, G. Delgado-Barrio, D. López-Durán, F. A. Gianturco, J. Jellinek, *Phys. Scr.* **2007**, *76*, C96.

[19] D. S. Miyoshi, R. M. Cotts, A. S. Greenberg, R. C. Richardson, *Phys. Rev. A* **1970**, *2*, 870.

[20] A. S. Dickinson, F. X. Gadéa, T. Leininger, *J. Phys. B At. Mol. Opt. Phys.* **2004**, *37*, 587.

[21] J. P. Toennies, A. F. Vilesov, *Angew. Chem. Int. Ed.* **2004**, *43*, 2622.

[22] Y. Moriwaki, N. Morita, *Eur. Phys. J. D* **2005**, *33*, 323.

[23] S. Grebenev, J. P. Toennies, A. F. Vilesov, *Science* **1998**, *279*, 2083.

[24] J. Harms, M. Hartmann, B. Sartakov, J. P. Toennies, A. F. Vilesov, *J. Chem. Phys.* **1999**, *110*, 5124.

[25] U. Even, I. Al-Hroub, J. Jortner, *J. Chem. Phys.* **2001**, *115*, 2069.

[26] T. Sternfeld, R. E. Hoffman, M. Saunders, R. J. Cross, M. Syamala, M. Rabinovitz, *J. Am. Chem. Soc.* **2002**, *124*, 8786.

[27] R.-F. Peng, S.-J. Chu, Y.-M. Huang, H.-J. Yu, T.-S. Wang, B. Jin, Y.-B. Fu, C.-R. Wang, *J. Mater. Chem.* **2009**, *19*, 3602.

[28] Y. Morinaka, S. Sato, A. Wakamiya, H. Nikawa, N. Mizorogi, F. Tanabe, M. Murata, K. Komatsu, K. Furukawa, T. Kato, et al., *Nat. Commun.* **2013**, *4*, 1554.

[29] G. R. Bacanu, T. Jafari, M. Aouane, J. Rantaharju, M. Walkey, G. Hoffman, A. Shugai, U. Nagel, M. Jiménez-Ruiz, A. J. Horsewill, et al., *J. Chem. Phys.* **2021**, *155*.

[30] L. Pang, F. Brisse, *J. Phys. Chem.* **1993**, *97*, 8562.

[31] M. Straka, J. Vaara, *J. Phys. Chem. A* **2006**, *110*, 12338.

[32] A. Krapp, G. Frenking, *Chem. Eur. J.* **2007**, *13*, 8256.

[33] E. Cerpa, A. Krapp, R. Flores-Moreno, K. J. Donald, G. Merino, *Chem. Eur. J.* **2009**, *15*, 1985.

[34] A. A. Popov, S. Yang, L. Dunsch, *Chem. Rev.* **2013**, *113*, 5989.

[35] J. Vicha, J. Vaara, M. Straka, *Phys. Chem. Chem. Phys. .* **2023**, *25*, 10620.

[36] S. Jalife, J. Arcudia, S. Pan, G. Merino, *Chem. Sci.* **2020**, *11*, 6642.

[37] S. Osuna, M. Swart, M. Solá, *Chem. Eur. J.* **2009**, *15*, 13111.

[38] M. Khatua, S. Pan, P. K. Chattaraj, *Chem. Phys. Lett.* **2014**, *610*, 351.

[39] P. Å. Malmqvist, *Int. J. Quantum Chem.* **1986**, *30*, 479.

[40] A. J. W. Thom, M. Head-Gordon, *J. Chem. Phys.* **2009**, *131*.

[41] E. J. Sundstrom, M. Head-Gordon, *J. Chem. Phys.* **2014**, *140*.

[42] J. H. Skone, M. V. Pak, S. Hammes-Schiffer, *J. Chem. Phys.* **2005**, *123*.

[43] P. Jungwirth, A. I. Krylov, *J. Chem. Phys.* **2001**, *115*, 10214.

[44] F. A. Gianturco, F. Paesani, I. Baccarelli, G. Delgado-Barrio, T. González-Lezana, S. Miret-Artés, P. Villarreal, G. Bendazzoli, S. Evangelisti, *J. Chem. Phys.* **2001**, *114*, 5520.

[45] A. Heidenreich, U. Even, J. Jortner, *J. Chem. Phys.* **2001**, *115*, 10175.

[46] D. López-Durán, M. P. de Lara-Castells, G. Delgado-Barrio, P. Villarreal, C. Di Paola, F. A. Gianturco, J. Jellinek, *Phys. Rev. Lett.* **2004**, *93*, 53401.

[47] M. de Lara-Castells, D. López-Durán, G. Delgado-Barrio, P. Villarreal, C. Di Paola, F. A. Gianturco, J. Jellinek, *Phys. Rev. A* **2005**, *71*, 033203.

[48] M. P. de Lara-Castells, G. Delgado-Barrio, P. Villarreal, A. O. Mitrushchenkov, *J. Chem. Phys.* **2006**, *125*, 221101.

[49] M. P. de Lara-Castells, R. Prosmiti, D. López-Durán, G. Delgado-Barrio, P. Villarreal, F. A. Gianturco, J. Jellinek, *Int. J. Quantum Chem.* **2007**, *107*, 2902.

[50] M. de Lara-Castells, P. Villarreal, G. Delgado-Barrio, A. O. Mitrushchenkov, *J. Chem. Phys.* **2009**, *131*.

[51] M. de Lara-Castells, A. O. Mitrushchenkov, G. Delgado-Barrio, P. Villarreal, *Few-Body Syst.* **2009**, *45*, 233.

[52] A. Valdés, R. Prosmiti, P. Villarreal, G. Delgado-Barrio, *J. Phys. Chem. A* **2012**, *116*, 7169.

[53] N. F. Aguirre, P. Villarreal, G. Delgado-Barrio, A. O. Mitrushchenkov, M. P. de Lara-Castells, *Phys. Chem. Chem. Phys* **2013**, *15*, 10126.

[54] M. P. de Lara-Castells, A. O. Mitrushchenkov, *Phys. Chem. Chem. Phys.* **2021**, *23*, 7908.

[55] C. G. Joslin, C. G. Gray, J. D. Goddard, S. Goldman, J. Yang, J. D. Poll, *Chem. Phys. Lett.* **1993**, *213*, 377.

[56] C. G. Joslin, J. Yang, C. G. Gray, S. Goldman, J. D. Poll, *Chem. Phys. Lett.* **1993**, *208*, 86.

[57] M. Zhang, L. B. Harding, S. K. Gray, S. A. Rice, *J. Phys. Chem. A* **2008**, *112*, 5478.

[58] M. Xu, F. Sebastianelli, Z. Bacic, R. Lawler, N. Turro, *J. Chem. Phys.* **2008**, *129*, 64313.

[59] S. Mamone, M. Ge, D. Hüvonen, U. Nagel, A. Danquigny, F. Cuda, M. C. Grossel, Y. Murata, K. Komatsu, M. H. Levitt, Others, *J. Chem. Phys.* **2009**, *130*, 81103.

[60] M. Xu, F. Sebastianelli, B. R. Gibbons, Z. Bacic, R. Lawler, N. J. Turro, *J. Chem. Phys.* **2009**, *130*, 224306.

[61] A. W. Hauser, A. O. Mitrushchenkov, M. P. de Lara-

Castells, *J. Phys. Chem. C.* **2017**, *121*, 3807.
[62] A. Szabo, N. Ostlund, *Modern Quantum Chemistry: Introduction to Advanced Electronic Structure Theory*, Dover Books on Chemistry, Dover Publications **2012**.
[63] P.-O. Löwdin, *Phys. Rev.* **1955**, *97*, 1474.
[64] K. Patkowski, G. Murdachaew, C. M. Fou, K. Szalewicz, *Mol. Phys.* **2005**, *103*, 2031.
[65] J. Charry, E. Posada, F. Moncada, J. Romero, A. Reyes, openLOWDIN v1.0.0 10.5281/zenodo.8125056 **2023**.
[66] E. F. Valeev, Libint: A library for the evaluation of molecular integrals of many-body operators over Gaussian functions, http://libint.valeyev.net/ **2022**, version 2.8.0.
[67] V. I. Lebedev, *Comput. Math. Math. Phys.* **1976**, *16*, 10.
[68] R. Flores-Moreno, E. Posada, F. Moncada, J. Romero, J. Charry, M. Díaz-Tinoco, S. A. González, N. F. Aguirre, A. Reyes, *Int. J. Quantum Chem.* **2014**, *114*, 50.
[69] A. Reyes, F. Moncada, J. Charry, *Int. J. Quantum Chem.* **2019**, *119*, e25705.
[70] F. Neese, F. Wennmohs, U. Becker, C. Riplinger, *J. Chem. Phys.* **2020**, *152*.
[71] W. Humphrey, A. Dalke, K. Schulten, *J. Molec. Graphics* **1996**, *14*, 33.
[72] A. Reyes, M. V. Pak, S. Hammes-Schiffer, *J. Chem. Phys.* **2005**, *123*, 64104.
[73] H. Bethe, *Ann. Phys.* **1929**, *395*, 133.
[74] U. Walter, *Phys. Rev. B* **1987**, *36*, 2504.
[75] S. Gómez, A. Restrepo, *Phys. Chem. Chem. Phys.* **2019**, *21*, 15815.
[76] P. M. Felker, Z. Bačić, *J. Chem. Phys.* **2020**, *152*.
[77] O. Carrillo-Bohórquez, Á. Valdés, R. Prosmiti, *J. Chem. Theory Comput* **2021**, *17*, 5839.